Composites Part A: Applied Science and Manufacturing,
Volume 37, Issue 2, CompTest 2004, February 2006, Pages 368-377.

Manuscript Number:

Title: Material characterisation and calibration of a meso- mechanical damage model for braid reinforced composites

Article Type: CompTest Conference Paper

Keywords:

Corresponding Author: Mr Michel Fouinneteau Cranfield University

Other Authors:

*** Manuscript**

Material characterisation and calibration of a meso-mechanical damage model for braid reinforced composites

A. K. Pickett & M. R. C. Fouinneteau

School of Industrial and Manufacturing Science, Cranfield University, Bedford, MK43 0AL, UK.

1. Abstract

Cost effective braid reinforced composites are a potential substitute for metals in many automotive structural applications where good mechanical performance combined with high energy absorption are of special interest. This paper presents experimental work undertaken to characterise braided composites and a meso- mechanical damage model suitable for the impact and crash analysis of braided composites. The model presented correctly represents stiffness, initial failure and the post failure damage response which is of particular importance for crash applications. Furthermore, work is presented that describes testing procedures which should be followed in order to obtain the correct material parameters for analysis. Finally, validation of the testing procedures and the constitutive model is made against a structural braid reinforced composite beam loaded to failure under four point bending.

Keywords Composites, Braided fabrics, Damage mechanics, Mechanical testing, Finite Element analysis

2. Introduction

In recent years cost effective advanced composites reinforced with Non Crimp Fabrics (NCF) and braids have received increased attention as possible materials for automotive, and other, applications. The CEC funded Framework VI project TECABS [1], for example, has recently combined both materials to successfully manufacture a large complex automotive floor assembly using RTM technology. Within the TECABS project braids were used for automotive side sills and have also been used for main rails in production vehicles [2]. Braids can be efficiently manufactured using rotary braiding machines which can be tailored to provide a wide variety of yarn architectures and preform shapes that are particularly suitable for closed form sectional members. Furthermore, the availability of new low cost carbon fibres and the use of flexible resin injection processes are helping to encourage industrial interest, particularly for low volume niche applications.

The particular class of composites considered here are carbon fibre reinforced braids for structural applications. Experimental work has shown that these materials offer a good compromise between mechanical performance, impact resistance and crash energy absorption. Under axial crushing of sectional members it is well known that composites can out perform metals for specific energy absorption [3]; braid reinforced composites are similarly competitive giving a two to three fold increase in specific energy absorption compared to metals for axial crushing of tubular sections [4].

However, braid reinforced composites can also absorb significant specific energy under tensile loading; for example, Figure 1 compares a [±45°] biaxial braid reinforced composite (67.2mm*1.6mm thick) and an automotive grade Aluminium 6014/T6 coupon (65.0mm*1.7mm thick) loaded to failure. Despite the lower ultimate strength of the composite the ability of the fabric architecture to reorientate enables large strains and high levels of energy to be absorbed over a much greater ‘non-local’ necking zone; Figure 2. In terms of specific energy absorption the 220 mm long braided composite achieves 9.16J/g compared to 4.16J/g for the Aluminium coupon. This superior performance could be advantageous in applications such as automotive side intrusion where large amounts of energy must be absorbed.

Most analytical constitutive models for advanced composites have been specifically developed for unidirectional (UD) plies and a large number of failure models are to be found in the literature [5]. Under impact and crash loading the limited models available, for example [6,7] usually treat the progressive composite fracture process using 'continuum damage mechanics' but, again, most models to date concern UD composites. The focus of this paper is testing methods specific to the characterisation of braid reinforced composites and their representation in a meso- mechanical damage model suitable for impact and crash simulation. In addition to braids, however, other more conventional composites will also be used to introduce some specific features of the meso- mechanical damage law.

3. The meso- mechanical damage model

The Finite Element (FE) code used for this work is a commercial explicit code [8] which has recently added new composite ply and delamination models based on damage mechanics [9]. For representation of each ply the original model proposed by Ladevèze [6] for UD composites is available and considers each elementary-ply at the macro- level as an orthotropic homogeneous material; continuum damage mechanics is used to treat strength degradation and failure. The principle ply failure mechanisms are fibre failure due to longitudinal tension or compression loading, resin micro-cracking due to transverse tension and fibre-matrix debonding due to shear loading. These failure modes can develop independently, or simultaneously, depending on the state of loading. The simplified plane stress orthotropic constitutive law with damage parameters is given by,

$$\begin{Bmatrix} \varepsilon_{11} \\ \varepsilon_{22} \\ \varepsilon_{12} \end{Bmatrix} = \begin{bmatrix} \frac{1}{E_1(1-d_1)} & \frac{-\nu_{12}}{E_1} & 0 \\ \frac{-\nu_{21}}{E_1} & \frac{1}{E_2(1-d_2)} & 0 \\ 0 & 0 & \frac{1}{G_{12}(1-d_{12})} \end{bmatrix} \begin{Bmatrix} \sigma_{11} \\ \sigma_{22} \\ \sigma_{12} \end{Bmatrix} = [S]\{\sigma\} , \qquad (3.1)$$

where the compliance matrix *[S]* comprises of four undamaged elastic constants E_1, E_2, G_{12} and υ_{12} and damage parameters d_1, d_2 and d_{12} for the two principle fibre and shear directions. Usually d_1 and d_2 are uncoupled, but there can be an interaction between d_2 and d_{12}. The mechanical and damage properties in tension and compression may be different.

The constitutive damage law uses internal damage variables to control material stiffness reduction and also to define failure. These variables must be calibrated against appropriate coupon tests which include the principle fibre [0°] and transverse [90°] directions under tension and compression, a shear test [±45°] and an additional test [±67.5°] designed to account for interaction of certain failure modes. The original Ladevèze model [6] demonstrated parameter identification for UD composites T300/914 and IM6/914. Investigations by the authors have found that tensile and compressive aspects of this model appear valid for a wide range of composite types; however, the shear response has limitations and improvements are proposed in the following section.

3.1 Shear mechanical testing and parameter identification for a UD Composite

The following describes shear [±45°] testing and parameter identification for a relatively ductile high strength UD carbon fibre composite, T800S/M21 manufactured by Hexcel [10]. The shear response of this material exhibits large strain and non-linear damage evolvement to failure and is useful to illustrate limitations and improvements to the model. The growth of shear damage is characterised using cyclic tensile testing on a [±45°] coupon; the damaged modulus at any instance is provided by the unloading modulus of the shear stress-strain curve, Figure 3. The modulus must be determined from stress and strain measures in the local lamina frame. The following expressions transform quantities between the loading frame (x,y) and the required local lamina frame (1,2).

$$\begin{cases} \sigma_{12} = \dfrac{\sigma_x}{2} \\ \gamma_{12} = 2\varepsilon_{12} = (\varepsilon_x - \varepsilon_y)\ , \end{cases} \tag{3-2}$$

The following identification of damage parameters follows the procedure outlined in [6] using the results from Figure 3. At each cycle the elastic and plastic strain components are available and are used to determine the damage and plasticity laws respectively. At least 5-6 cycles are required to obtain a good evolution of damage and plasticity.

The damage law: The damaged shear modulus at each cycle is given by,

$$\mathrm{d}_{12} = 1 - \frac{\mathrm{G}_{12}}{\mathrm{G}^{0}_{12}} \ , \tag{3-3}$$

where G_{12} is the damaged modulus and G^0_{12} is the initial undamaged value. The elastic strains ε^e_{12} are used to compute the conjugate shear forces $\underline{Y}_{12}$ at each cycle from,

$$\underline{\mathrm{Y}}_{12} = \sqrt{\frac{1}{2}\mathrm{G}^{0}_{12}(2\varepsilon^{\mathrm{e}}_{12})^{2}} \ . \tag{3-4}$$

Conjugate forces are 'driving forces' that govern damage propagation. Figure 4 shows the experimental points relating evolution of conjugate forces $\underline{Y}_{12}$ and damage d_{12}. Reference [6] assumes a linear relationship between these two quantities given by,

$$\underline{Y}_{12}(d_i) = Y_{12C}\, d_i + Y_{120} \ , \tag{3-5}$$

from which the parameters Y_{12C} and Y_{120} for the linear damage law can be identified, Figure 4. A final damage constant Y_{12R} denoting ultimate failure is found by specifying the maximum damage value d_{sat} in equation (3-5).

The plasticity law: Parameters for the plasticity law are derived from the evolution of plastic strains at each cycle. The plasticity hardening function $R(p)$ is derived from (3-6) and (3-7). A fitting procedure is used to define a power law having three constants; namely, the initial yield stress R_0 and the hardening coefficients β and α.

$$f_p(\tilde{\sigma}, R) = \frac{\sigma_{12}}{1 - d_{12}} - R(p) - R_0 = 0 \tag{3-6}$$

$$p = \int_0^{2\varepsilon^p_{12}} 2\,(1 - d_{12})\, d\varepsilon^p_{12} \tag{3-7}$$

The shear damage and plasticity constants assuming a linear damage function are given in Table 1.

It is evident from Figure 4 that the original linear damage law proposed by Ladevèze [6], equation (3.5), cannot represent the latter stages of damage and, in particular, the ultimate

failure condition. This nonlinear failure behaviour has been observed by the authors for a number of woven, Non Crimp, and braided composites which have relatively ductile matrices and allow considerable fibre rotation in shear prior to failure. Consequently, alternative laws describing the evolution of $\underline{Y}_{12}$ and d_{12} are proposed as shown in Figure 4. These are; namely, a linear, logarithmic and polynomial function of rank 2. The logarithmic function was previously proposed by Johnson and Pickett [11] for woven fabric composites.

Figure 5 shows the consequence of these three damage functions on the shear stress strain relation. The linear function cannot represent the experimental trend and predicts premature failure; the logarithmic function gives an improved correlation, but clearly the polynomial function gives the best agreement and estimate for failure strain.

4. Braided composites

Mechanical properties for constitutive models to be used in Finite Element analysis are usually determined from appropriate regulatory tests; for example, the ASTM standards D3410/D [12] and D3518/D [13] for tensile and compression testing respectively. However, braided composites do have some particular features that should be noted in the testing programme. First, most braided composites have a continuous architecture without free edges, whereas coupon testing is usually performed on specimens cut from flat panels and therefore having free edges. Second, in the case of multi-layer braids, there is a thickness effect that should be considered. Section 4.1 discusses the damage mechanisms that occur in biaxial braids under tensile loading. This is then followed by experimental work to investigate the effects that free edges and the number of layers have on composite mechanical properties.

4.1 The damage mechanisms and fibre rotation

For biaxial [$\pm\theta°$] braids under tensile loading the damage development has been shown to be nonlinear, Figure 4, and is due to matrix micro-cracking and plasticity associated with large fibre rotation. The fibre/matrix interface progressively debonds allowing tows to align; this scissor action continues until the tows reach a maximum interlocking angle and rupture, or the fibre start to fail due to the loss of integrity and the large shear strains. This

behaviour is illustrated in Figure 6 for a tensile loaded $[\pm 45^\circ]_{4s}$ braid where significant fibre matrix debonding and tow alignment has occurred leading to significant necking prior to failure of the specimen.

Delamination between plies is a further damage mechanism that has been observed in multi-layered braid composites, Figure 7. This damage mode is due to the shearing deformation and is strongly coupled to the ply damage mechanism. This failure leads to separation of the plies and will reduce the ability of the laminate to sustain bending loads. Characterisation of this failure mode has not been treated here and will be investigated in future work.

4.2 The edge effect: Cut and uncut coupons

A test program was undertaken to determine the difference between mechanical properties and failure for coupons having cut and uncut edges. The work used 40mm diameter braids with 24K STS tows and 42 ends manufactured by Eurocarbon, the resin/hardener was LY3505/XB3403 from Huntsman Advanced Materials. All coupons were manufactured using the VARI process which gave a fibre volume ratio of 53%. Two fabric architectures have been considered; namely, a $[\pm 25]_{4S}$ and a $[\pm 45]_{4S}$ braid.

The tubular braids were carefully flattened in order to maintain the fabric architecture prior to impregnation. Figure 8 shows the flattening of the braids which were either cut after curing, or left intact, to provide the two types of edge conditions. Due to the relatively coarse architecture of the braid having a 'Repetitive Unit Cell' (RUC) of 14 mm square it was decided to use test coupons of 65mm width; this is in line with reference [14] which recommends that specimen width is at least three times the RUC to ensure a uniform strain distribution.

For the $[\pm 25]_{4S}$ braided composite the cut and uncut coupons had identical initial mechanical properties (E_o); however, the uncut coupons showed significantly greater ultimate load (+27.5%) and strain to failure (+39.1%) as shown in Figure 9. and Table 2. The observed failure modes are also shown in Figure 9 and are similar for the two types of specimens. The loss of tow continuity in the cut specimen leads to a combination of tow

pull-out and tow failure which initiate at the free edges; whereas, for the uncut specimen tow breakage initiates at the area of highest stress concentration adjacent to the tabs.
A second study is presented in Figure 10 for the $[\pm 45]_{4S}$ cut and uncut braid reinforced composite. In this case a similar trend is observed to the previous $[\pm 25]_{4S}$ case, except that the difference between cut and uncut strength is reduced to 13,3%. This is due to the increased transfer of load by transverse matrix mechanisms rather than fibre mechanisms; thus the anchorage effect of the fibres at the edges is less significant.

This brief study indicates that braid angle strongly influences the strength between 'cut' and 'uncut' braid reinforced coupons. It shown that failure in biaxial 'open' braids, which are dominated by transverse matrix failure, does not greatly affect the failure strength using the two edge conditions. Whereas for low angle braids the load transfer mechanisms are fibre dominated and the difference between 'cut' and 'uncut' edge condition is much greater. The width of the coupon tested can also be expected to influence these trends. It may be concluded that mechanical data obtained from cut coupons should be used with caution for the FE analysis of closed sectional members. Conversely, cut edges in a braided structure should have mechanical data obtained from corresponding 'cut' coupon tests.

Figure 10 shows the damage development for the $[\pm 45]_{4S}$ coupons presented in Figure 10 with cut and uncut edge conditions. It can be seen that both coupon types have similar damage evolution, at least to the point where strain gauge measurements were possible at about 5% strain.

4.3 Influence number of layers on composite strength for braids

A further variable that influences braid mechanical properties is the number of plies. Laminates having only a few plies tend to have distinct resin rich pockets between fabric tows, Figure 12. As additional plies are added these areas are displaced with tows from the overlaid plies leading to greater material homogeneity. The affect on mechanical properties is investigated for four [±45°] braids having cut edges with 1, 2, 4 and 6 layers.

Cyclic loading has been applied to determine the damage and hardening laws for each lay up. Figure 13 shows that the number of plies does not appear to influence the damage law; however, it does have a significant effect on the hardening law, Figure 14. The hardening law shows that a single ply exhibits significantly more deformation compared to the other layups probably due to the higher void content allowing greater freedom for fabric deformation. For laminates with two or more plies the plasticity law starts to be consistent. Again, however, it must be noted that these observations are for test measurement conducted to only about 5% strain which was the limit of the strain gauges. It has also been observed that braids with low ply numbers are liable to fail at a slightly lower failure strain, probably due to inconsistencies in the fabric architecture.

5. Example for the loading of a braid reinforced beam

Figure 15 shows the experimental test setup for the braid reinforced beam having dimensions 1100mm long by 60mm square cross section. The braided beam uses a $[\pm 45^\circ]_{4S}$ architecture and the previously cited fibre and resin systems. Different braided beams have been considered having alternative inner structures; for example an open square section and a 2*2 cell section as shown in Figure 16. In each case the beams have been loaded to failure under static four point bending.

Results for the beam study are presented in Figure 16 and compare the FE simulations using linear and polynomial damage functions with test measurements. In this case a polynomial function of rank 3 has been used to capture the relationship between conjugate forces $\underline{Y_{12}}$ and damage d_{12}; the higher order polynomial is needed to capture the experimental points $(\underline{Y_{12}}, d_{12})$ and also allow rapid damage growth after damage saturation is reached, this polynomial form is shown schematically in Figure 4. The linear damage function predicts, as expected, premature failure of the beam, whereas the improved polynomial function gives an encouraging agreements with test results.

5. Conclusions

A meso-scale damage model has been adapted and presented for braid reinforced composites. Experiments have shown that biaxial braid reinforced composites can undergo large shear deformations and associated fibre rotations leading to a non-linear evolution of damage. Alternative shear damage laws have been proposed and a good agreement between test measurements and the law using a higher order polynomial function has been found. However, difficulties have been encountered to accurately measure strains the latter stages of shear deformations and further work will be needed to validate the model in this region.

The failure analysis of a braided composite structure requires correct interpretation of coupon test measurements. Work has been presented showing the important effect that the edge condition (cut or uncut) of a tensile coupon has on failure load. It has been shown that uncut continuous braids give significantly greater strength and strain to failure and that this is dependent on the braid angle. The influence of the number of plies is a further important material variable that must be taken into consideration in the parameter identification process. A FE analysis of a braided composite beam has given encouraging agreement between test and simulation results using the new braid meso-scale damage model and mechanical data obtained from appropriate mechanical testing.

6. References

1. Technologies for carbon fibre modular automotive Body Structures, Framework V project G6RD-CT2001-00636, http://www.tecabs.org, 1998-2002.
2. Mercedes Benz SLR McLaren: Technology for the 21st Century, AutoTechnology, 5/2003, p28-31.
3. Hull D. A unified approach to progressive crushing of composite tubes, Composites Sci Tech, 40, p377-421.
4. De Blic A. Performance car crash energy management structures, MSc individual thesis, Cranfield University, 2003.

5. Hinton MJ, Kaddour AS, Soden PD. A comparison of the predictive capabilities of current failure theories for composite laminates, judged against experimental evidence, Composite Science and Technology, Vol. 62, Issues 12-13, September-October 2002, p1725-1797.
6. Ladevèze P, Le Dantec E. Damage modelling of the elementary ply for laminated composites. Composites science and technology, 1992; 43: p.257-267.
7. Haug E, De Rouvray A. Crash response of composite structures. In Structural crashworthiness and failure, Ed. Jones N and Wierzbicki, Elsevier Applied Science, 1993, p237-294.
8. PAM-CRASH™ FE Code, Engineering Systems International, 20 Rue Saarinen, Silic 270, 94578 Rungis-Cedex, France.
9. Johnson AF, Pickett AK, Rozycki P. Computational methods for predicting impact damage in composite structures. Composites Science and Technology 2001; 61: p2138-2192.
10. Hexcel. http://www.hexcel.com.
11. Johnson AF, Pickett AK. Numerical modelling of composite structures under impact loads. In: Proceedings of DYMAT 2000 Conference. Krakow, September 2000.
12. ASTM. Standard test method for compressive properties of polymer matrix composite materials with unsupported gage section by shear loading. D 3410/D D3410M-95.
13. ASTM. Standard test method for in-plane shear response of polymer matrix composite materials by tensile test of a ±45° laminate. D 3518/D D3518M-94.
14. Minguet PJ, Fedro MK, Gunther CK. Test methods for textile composites. NASA CR 4609, 1994.

7. Figures

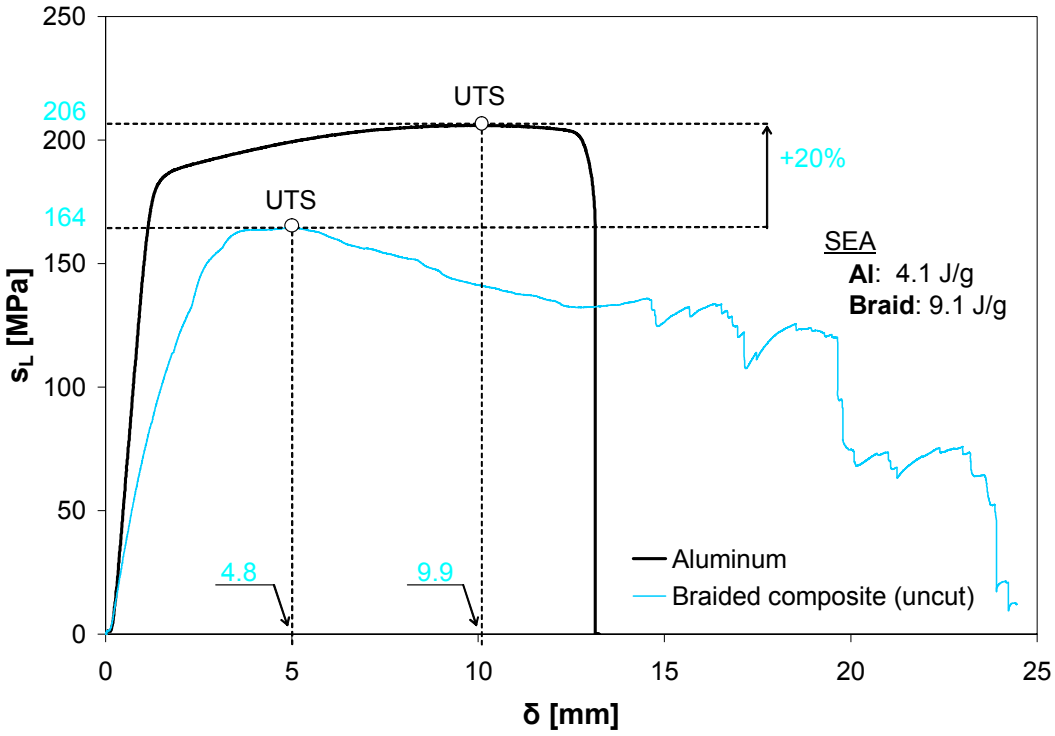

Figure 1. Engineering stress versus displacement for a bi-axial braid reinforced composite and Aluminium tensile coupon

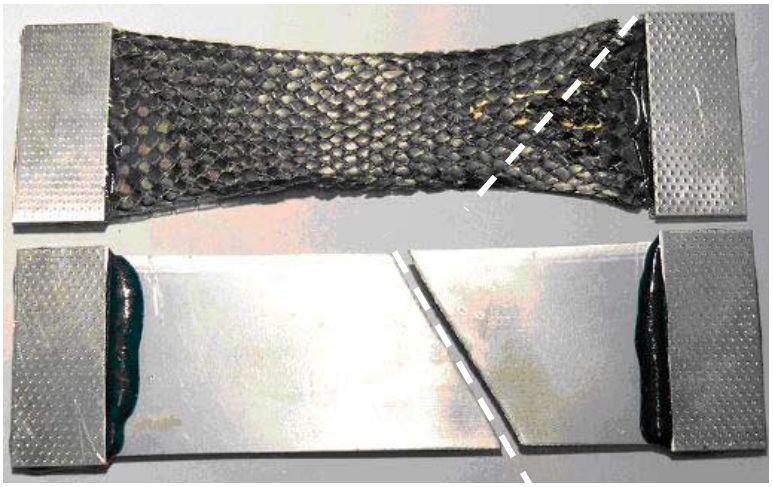

Figure 2. Comparison of failure mechanisms for a bi-axial braid reinforced composite and Aluminium tensile coupon

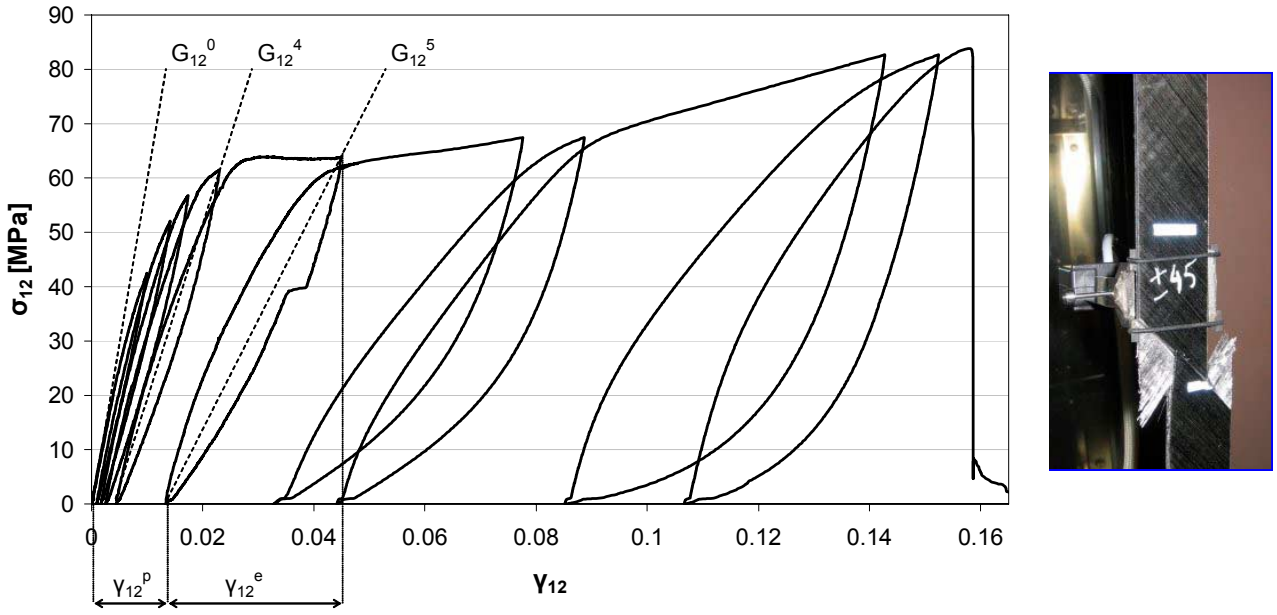

Figure 3. Shear stress (σ_{12}) versus shear strain (γ_{12}) showing cyclic loading for a $[\pm 45]_{4S}$ coupon of T800S/M21 and the failed specimen

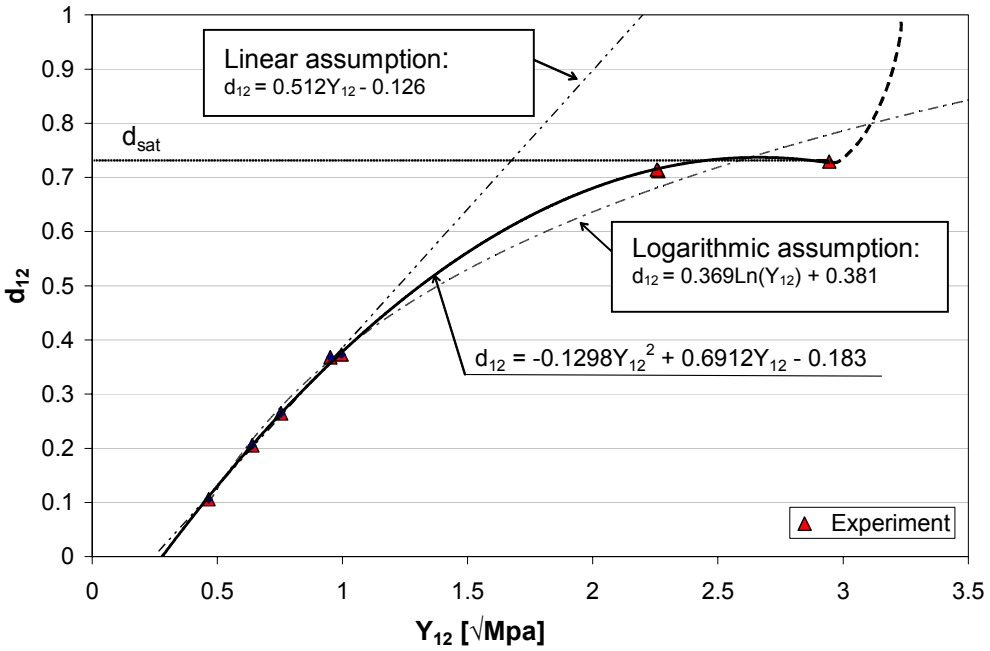

Figure 4. Experimental data points for Y_{12} and d_{12}, and alternative damage functions to relate these quantities

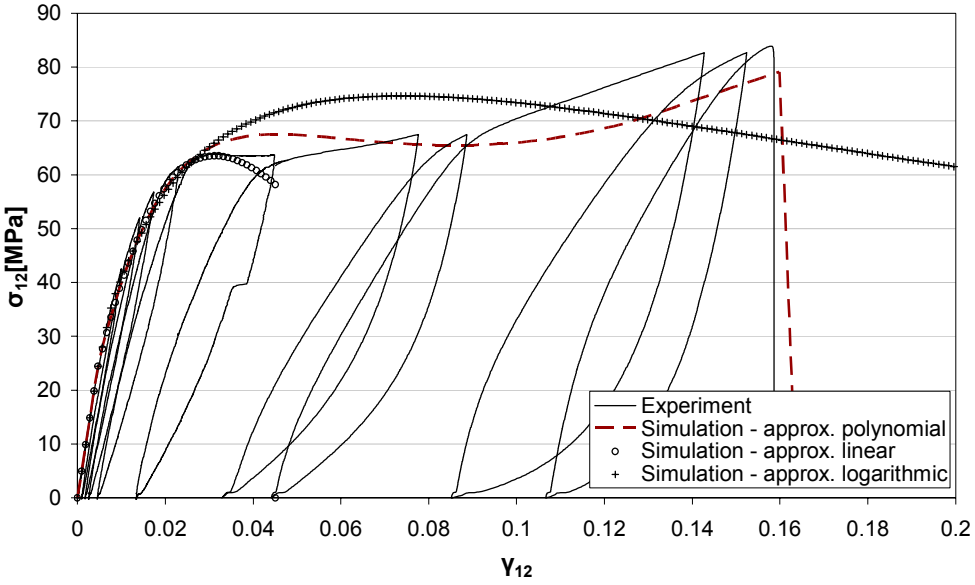

Figure 5. Experimental cyclic shear stress-strain curve for T800S/M21 composite and prediction using the three damage functions

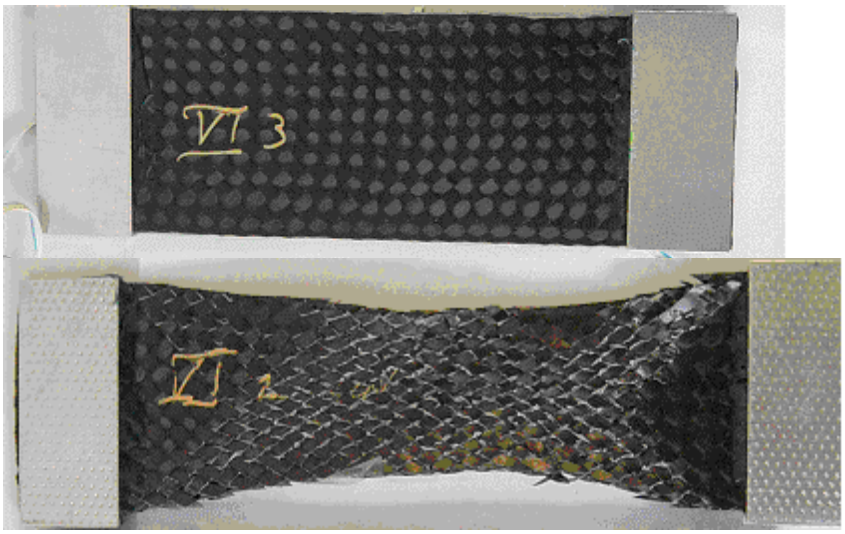

Figure 6. Deformation and failure mechanism for biaxial [±θ°] braid reinforced composite under tensile loading

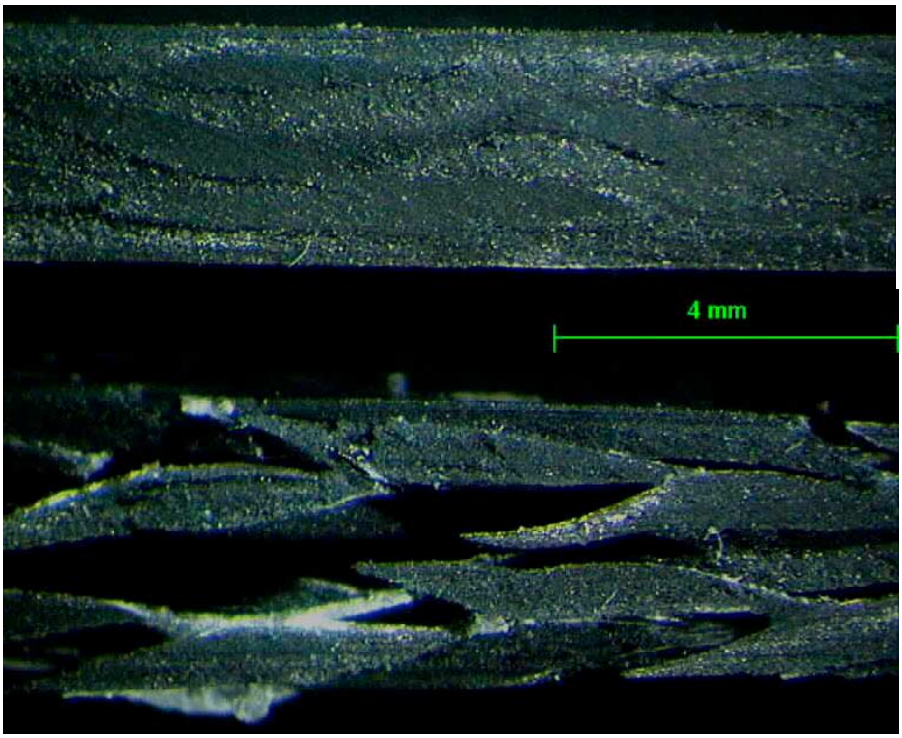

Figure 7. The original and delaminated braid reinforced composite

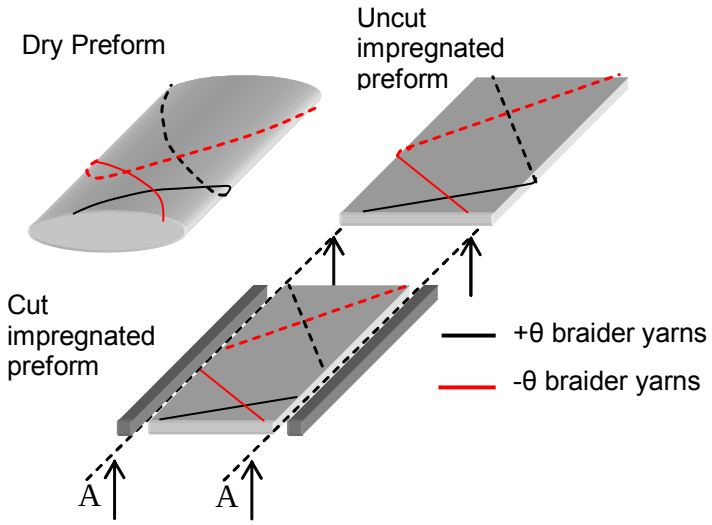

Figure 8. Preparation of the cut and uncut braid coupons

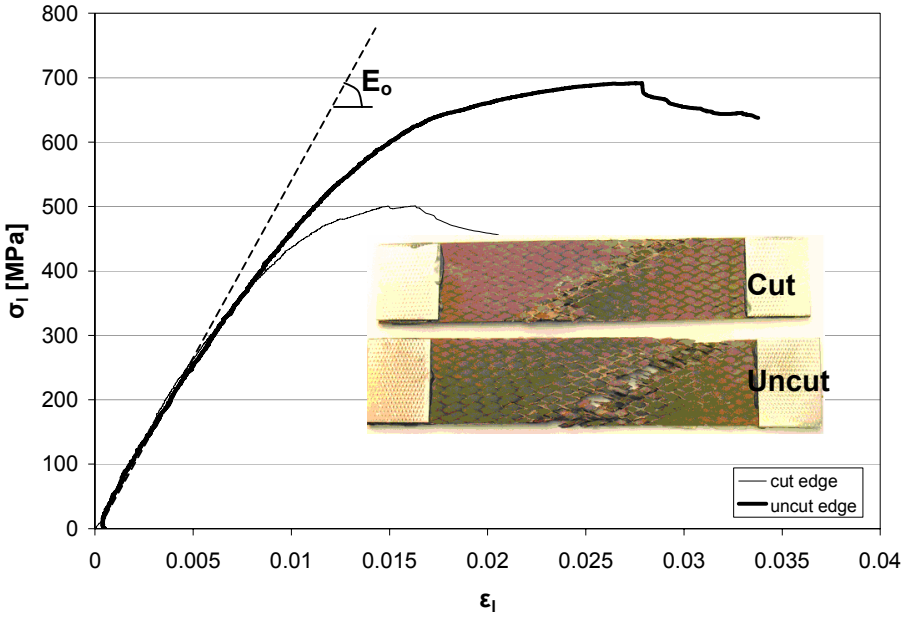

Figure 9. Comparison of results for the cut and uncut $[\pm 25]_{4S}$ braided coupons

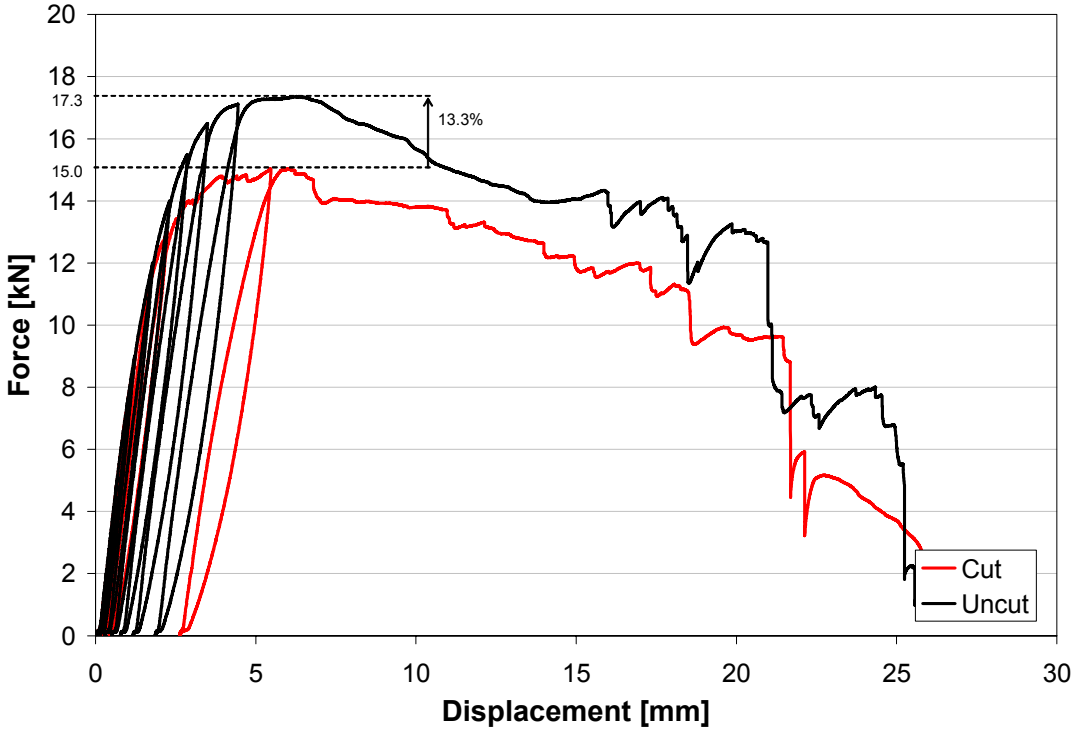

Figure 10 Force-Displacement curves for $[\pm 45]_{4S}$ cut and uncut coupons under tensile cyclic loading to failure

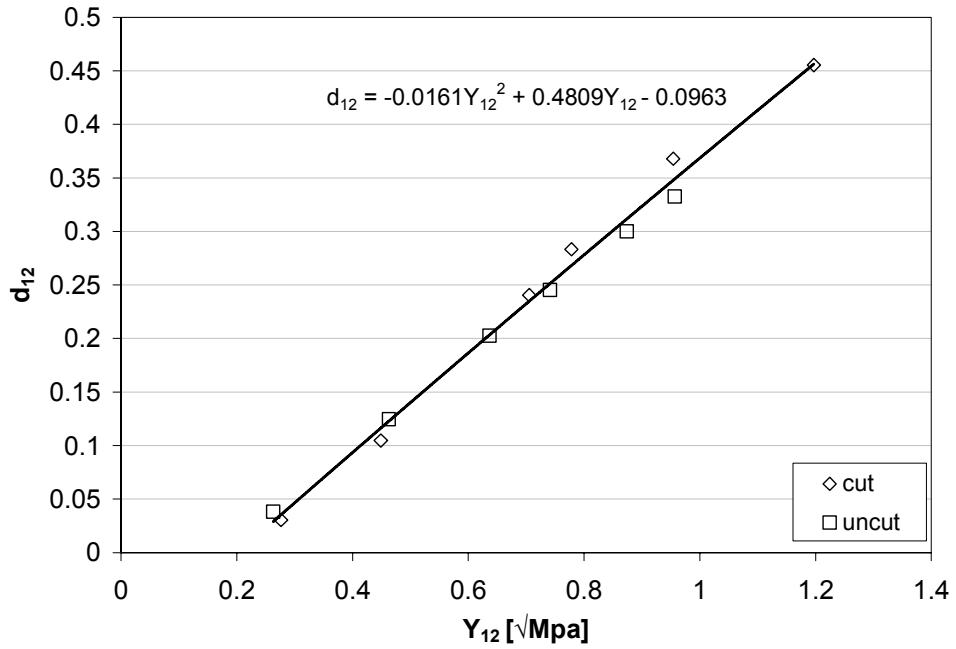

Figure 11 Damage laws for uncut and cut specimens

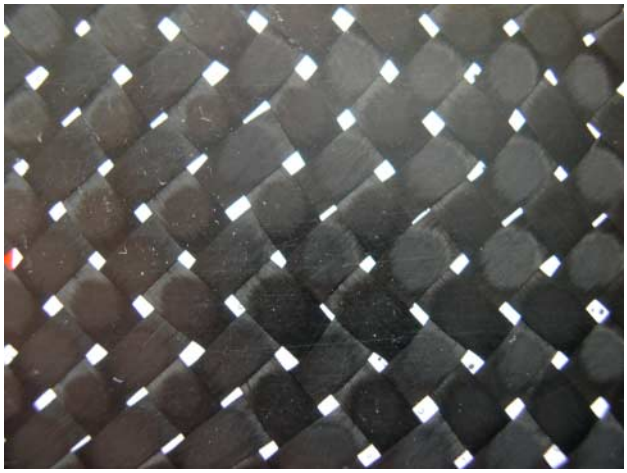

Figure 12 Fabric architecture and potential resin rich areas for a single layer braid

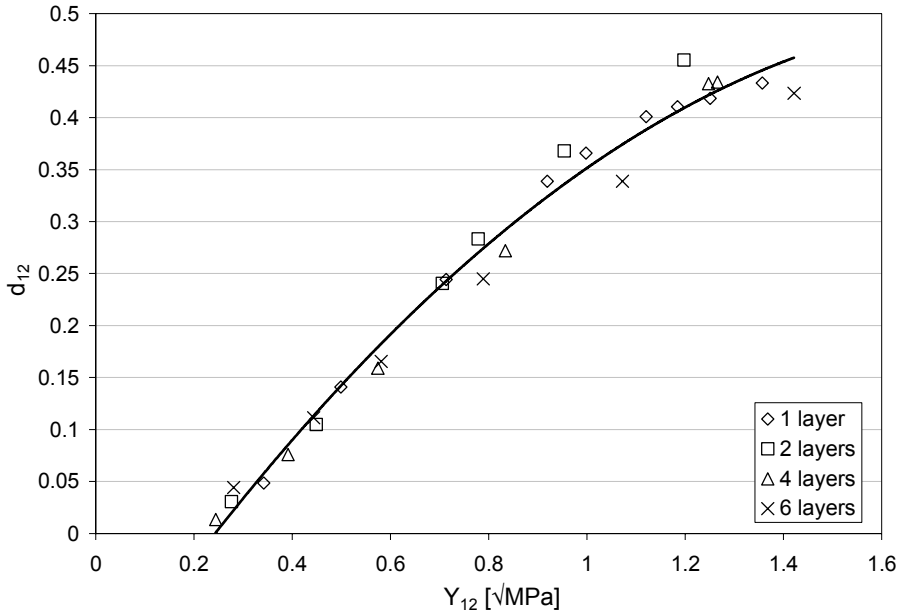

Figure 13. Damage laws for the different braid layups

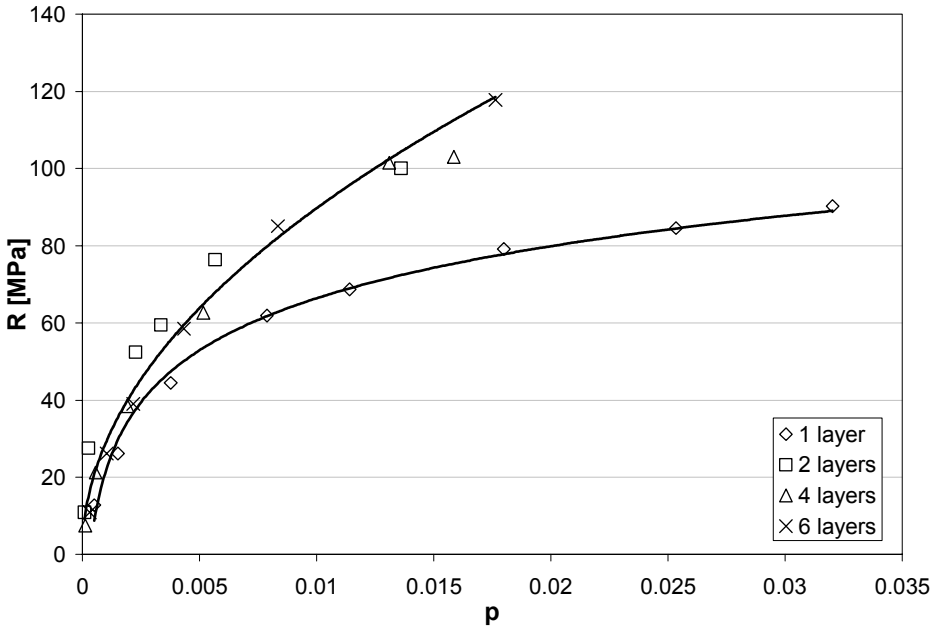

Figure 14. Hardening laws for the different braid layups

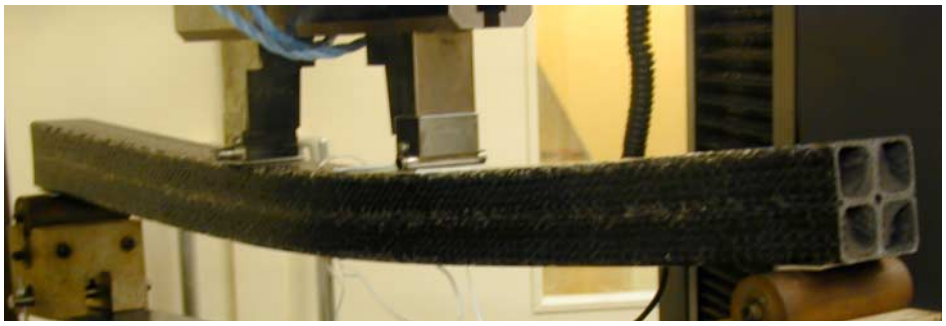

Figure 15 Braided beam using a 2*2 cell structure under 4 point bending

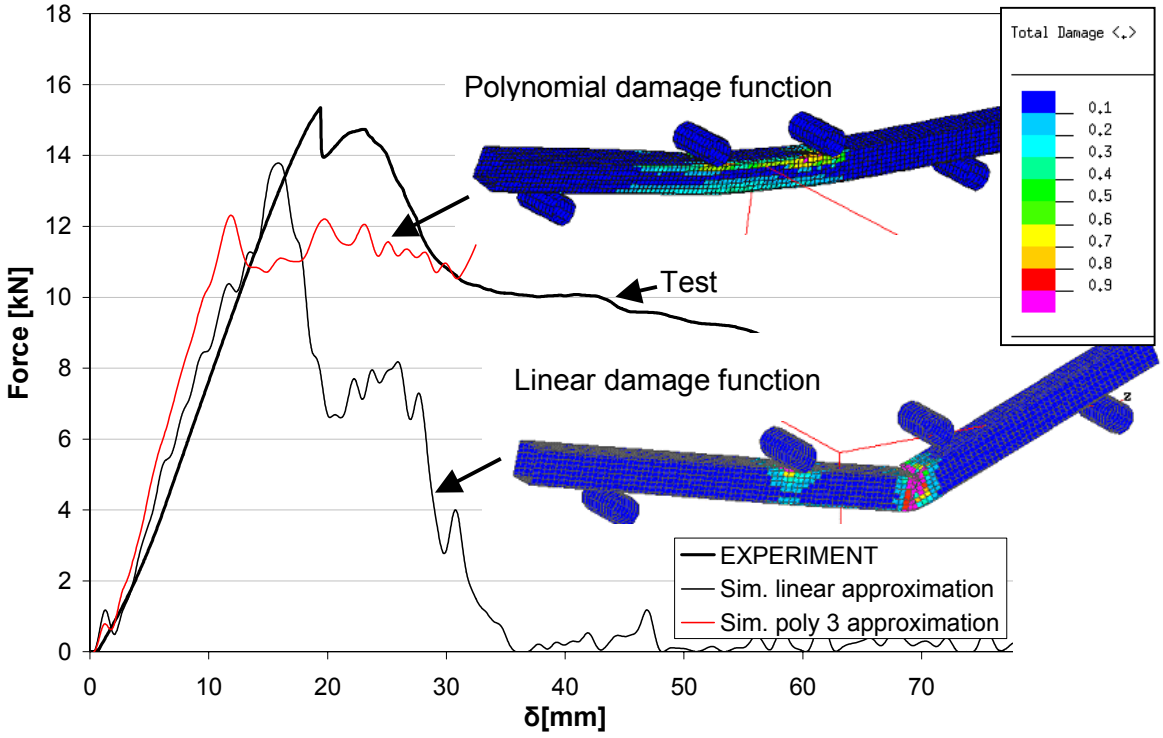

Figure 16. Simulation results for the four point loaded braid reinforced beam

8. Tables

Material constant for Hexcel T800S/M21		Value
G_{12}^{0}	Initial shear modulus in plane (1,2)	5259 (MPa)
Y_{12C}	Critical shear conjugate force	1.953 $(\sqrt{MPa})$
Y_{120}	Initial shear conjugate force	0.246 $(\sqrt{MPa})$
Y_{12R}	Shear conjugate force limit	1.416 $(\sqrt{MPa})$
d_{11u}^{t}	Damage saturation threshold	0.598
R_0	Initial yield stress	23.58 (MPa)
B	Hardening law multiplier	2356 (MPa)
A	Hardening law exponent	0.636

Table 1. Damage and plasticity law constants for a T800S/M21 composite

	$[\pm 25]_{4S}$ 24k STS fibre, 42 ends		
Property	*Cut*	*Uncut*	*Difference*
σ_{UTS} (MPa)	501	691	+27.5%
ε (failure)	0.02057	0.03379	+39.1%

Table 2. Comparison of mechanical properties for the cut and uncut $[\pm 25]_{4S}$ braided coupons